# Gated proton transport in aligned mesoporous silica films

RONG FAN[1], SEONG HUH[1], RUOXUE YAN[1], JOHN ARNOLD[1] AND PEIDONG YANG[1,2,3]*

[1]Department of Chemistry; [2]Department of Materials Science and Engineering, University of California; [3]Materials Science Division, Lawrence Berkeley National Laboratory, Berkeley, California 94720, USA

*e-mail: p_yang@berkeley.edu

Published online: 24 February 2008; doi:10.1038/nmat2127

**Modulated proton transport plays significant roles in biological processes[1] such as ATP synthesis[2,3] as well as in technologically important applications including, for example, hydrogen fuel cells[4,5]. The state-of-the-art proton-exchange membrane is the sulphonated tetrafluoroethylene copolymer Nafion developed by DuPont in the late 1960s, with a high proton conductivity[6]. However, actively switchable proton conduction, a functional mimic of the ion transport within a cell membrane, has yet to be realized. Herein, we report the electrostatic gating of proton transport within aligned mesoporous silica thin film. It is observed that surface-charge-mediated transport is dominant at low proton concentrations. We have further demonstrated that the proton conduction can be actively modulated by two–fourfold with a gate voltage as low as 1 V. Such artificial gatable ion transport media could have potential applications in nanofluidic chemical processors, biomolecular separation and electrochemical energy conversion.**

Nanofluidic systems have been attracting great interest owing to the emergence of novel ion transport properties and their promise in ultrasensitive detection of biomolecules. Ion transport through nanoscopic channels exhibits unique characteristics that differ significantly from bulk behaviour. Owing to the high surface-to-volume ratio of nanochannels, surface charges can completely govern ionic conductance such that the conductance can be enhanced by orders of magnitude, and seems independent of bulk ionic concentration[7,8]. Once the channel dimension falls into a characteristic length scale close to the Debye screening length ($L_d$), a unipolar ionic environment in which counter ions are highly enriched begins to emerge. A rich collection of phenomena, such as local ion depletion/enrichment[9], energy conversion from streaming current[10,11], rectified ion transport[12–16] and ionic current crossover on protein binding[17], have recently been observed on the basis of this effect. Moreover, through active tuning of surface charge density, the transport of ions, molecules or even proteins can be manipulated under fast electrostatic control[18–23]. However, for channels with dimensions of 10 nm and larger, a necessary condition for realizing a unique unipolar ionic environment is to work with a sufficiently low ionic strength; this is usually impractical in various applications, including separation of biomolecules in physiological media and ion transport in high-energy-density fuel cells or batteries. Accordingly, it is highly desirable to further shrink current nanofluidic devices down to sub-10 nm scales. With such a nanochannel dimension, a unipolar working condition could be achieved at realistic ionic concentrations (for example, ~0.1 M).

Conventional lithographical approaches have enabled the fabrication of nanochannels that are tens of nanometres in dimension, but intrinsic difficulties are encountered in making sub-10 nm nanofluidics[24–27]. Chemical synthesis, on the other hand, provides a practical alternative using self-assembled soft templates to produce nanoscopic porous inorganic materials[28,29]. Among these, mesoporous silica with uniform cylindrical nanochannels, for example, SBA-15 with its channel size of less than ten nanometres[30–32], could in principle serve as a good nanofluidic system. Herein, we report a dip-coating process for the alignment of uniform SBA-15 mesochannels (pore size < 8 nm) in thin-film form. We show that proton conductivity within these aligned nanochannels can be actively modulated in a two–fourfold range in a fast, reversible manner with an electric gate voltage as low as 1 V.

Aligned mesoporous silica (SBA-15) thin films were synthesized using a block-polymer-templated sol–gel process followed by controlled calcination (see the Supplementary Information). To obtain a well-aligned mesopore thin film for the proton transport study, several technical steps are essential. First, we exploited a controlled dip-coating process that yields aligned mesopore arrays[31]. In this process, the worm-like polymer micelles align along the direction of fluid motion and parallel to the substrate surface. Second, a slow, step-wise calcination is crucial to minimize the effect of thermal stress. Third, the film has to be sufficiently thin (typically 100–200 nm). The SBA-15 films consist of continuous mesochannels along the dip-coating direction, packed into a hexagonal two-dimensional lattice. Such mesopore alignment could be attributed to the interfacial shear at reduced dimension[33,34]. Figure 1a shows the small-angle X-ray diffraction spectrum of a calcined SBA-15 film, exhibiting a strong diffraction peak at 6.8 nm corresponding to the (100) lattice planes. The centre-to-centre distance of mesopores, $a_0$, is ~7.9 nm according to the (100) diffraction peak, which is in good agreement with reported values for SBA-15 mesostuctures[32]. The size of actual ion conduction channels will be less than 7.9 nm owing to finite wall thickness. High-resolution scanning electron microscopy imaging unambiguously demonstrates the formation of highly orientated nanochannels over a long range. Cross-sectional and top-view scanning electron micrographs (Fig. 1b,c) clearly shows the hexagonal packing of the nanopores aligned along the dip-coating direction. The top-surface feature (Fig. 1c) is reflective of long-range ordering of the mesochannels and their macroscopic alignment[35]. These mesopore thin films with long-range continuous nanochannels are ideal for the application of fluid and ion transport in this study.

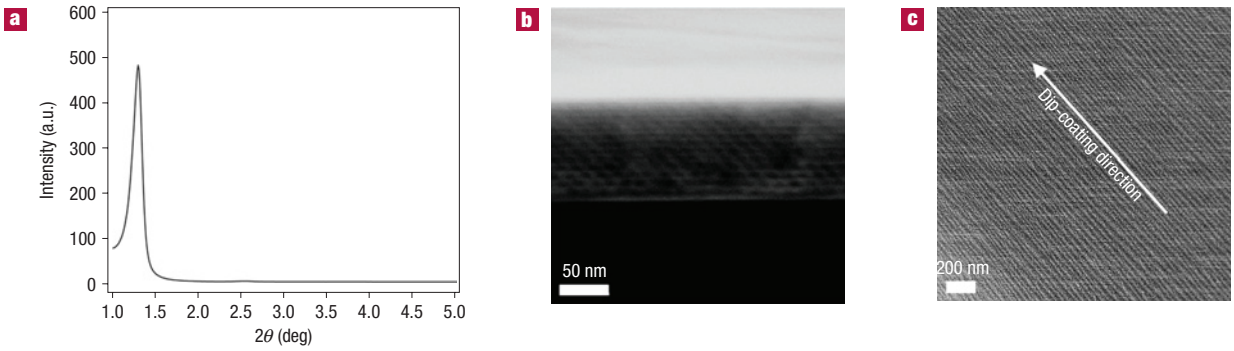


**Figure 1 Synthesis of large-scale aligned mesopore thin films. a**, Small-angle X-ray diffraction pattern recorded on the thin film. **b**, Scanning electron micrograph of the cross-section of a well-aligned mesopore thin film. **c**, Scanning electron micrograph of the top view of a well-aligned mesopore thin film.

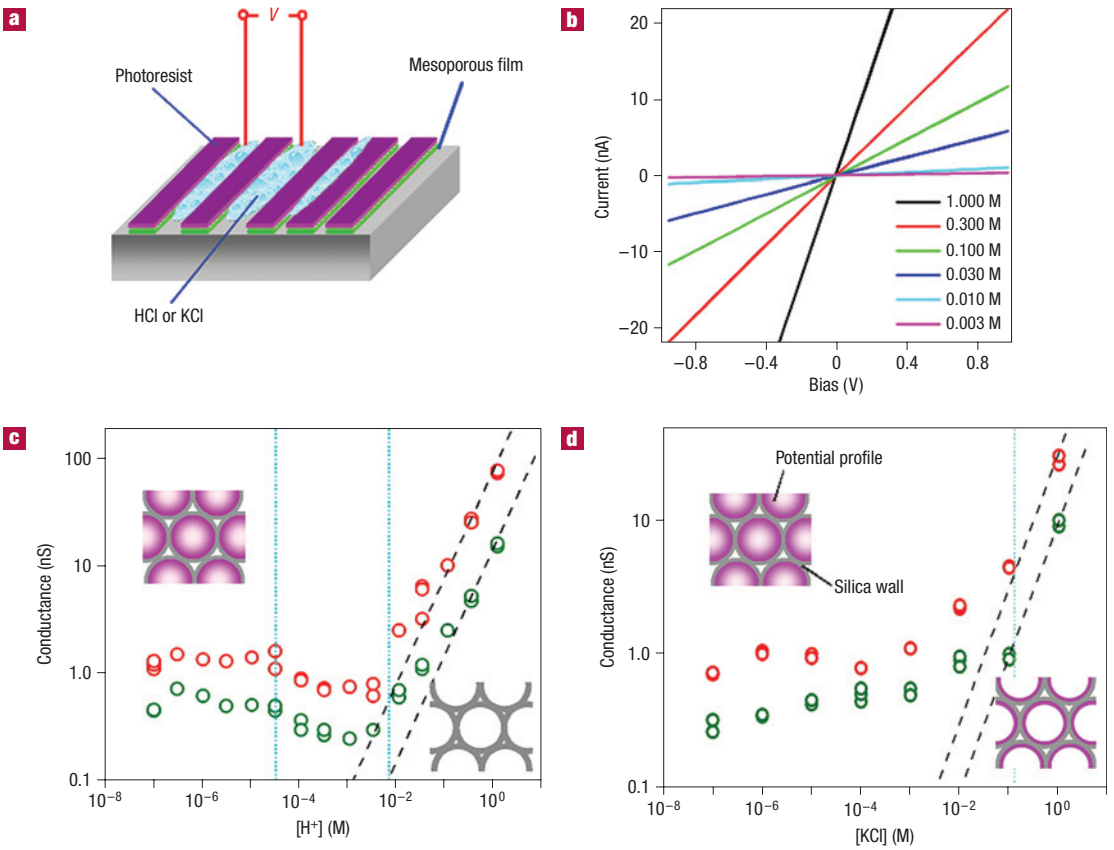


**Figure 2 Concentration dependence of proton and ion transport. a**, Schematic diagram of the measurement of ionic current through coarse-patterned mesopore thin-film stripes. **b**, Representative current/bias ($I$/ $V$) curves recorded at different proton concentrations. **c**, Proton concentration dependence of ionic conductance. It apparently deviates from bulk behaviour (dashed lines) at lower concentration and changes to a surface-governed ion transport. Proton conduction exhibits three distinct regions—a surface-charge dominant zone (lowest $[H^+]$), a bulk concentration dominant zone (highest $[H^+]$) and an intermediate zone where surface charge density is significantly reduced by increasing proton concentration resulting in a minimum of ionic current. High $[H^+]$ (beyond the isoelectric point, pH 2.6) results in a nearly zero surface potential owing to complete protonation. **d**, KCl salt concentration dependence of ionic conductance. The insets schematically show the electrostatic potential (magenta) within nanochannels. It extends well into the nanochannels at low concentrations owing to the large screening length, but becomes shielded at $[KCl] > 0.1$ M. Red and green circles in **c**,**d** represent data taken from two independent devices.

Proton conduction was first tested on macroscopic film patches that are defined by photolithography (see the Supplementary Information). As shown in Fig. 2a, the mesopore film stripes (green, ~2 mm in width) were created by reactive ion etching. Each of the stripes had a large number of nanochannels perpendicular to the stripe edge. On top of each stripe, a hard-baked photoresist

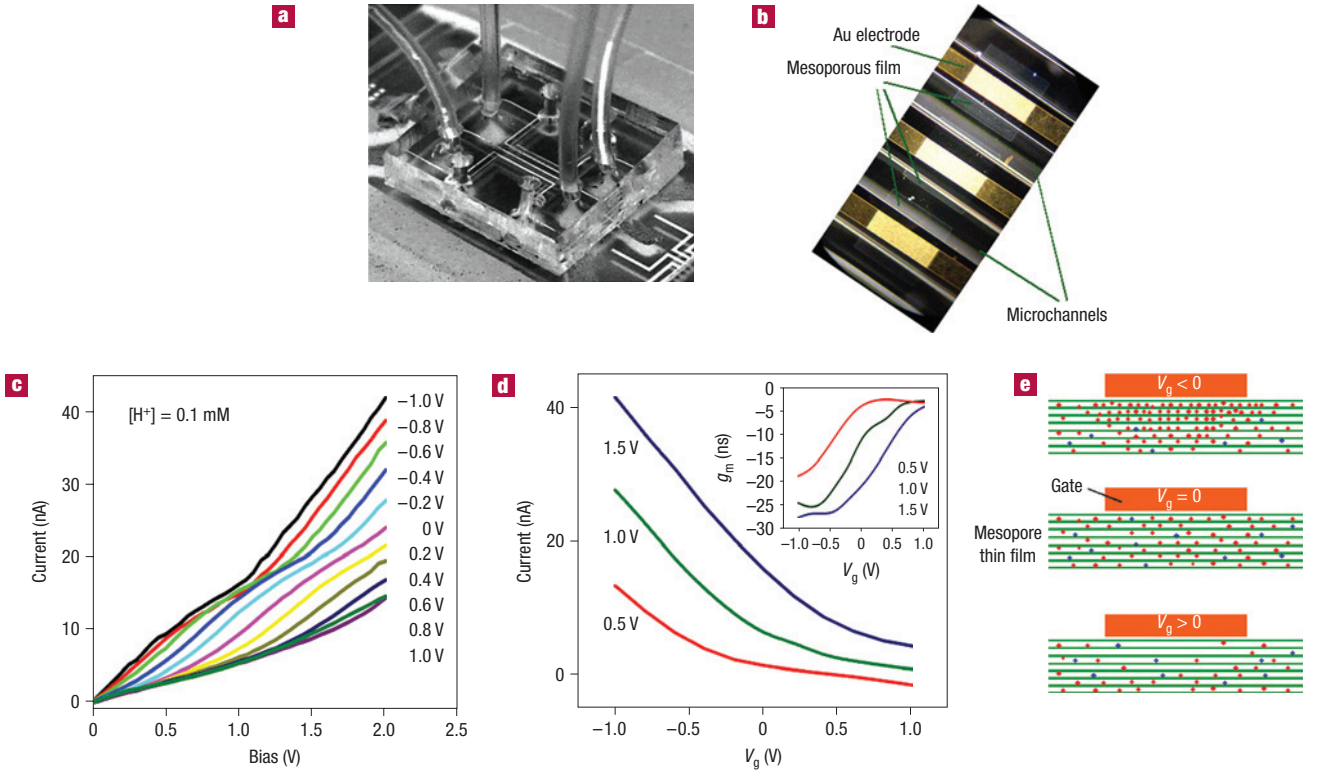


**Figure 3 Gate modulation of proton conduction. a**, Photograph of a mesopore thin-film nanofluidic device. **b**, Dark-field micrograph showing the layout of three mesopore thin-film patches, three gate electrodes made of sputtered Au and four microfluidic channels in a PDMS chip at the centre of the packaged nanofluidic device. **c**, Representative $I/V$ curves under gate voltages ranging from −1 to +1 V. Zero shift has been subtracted. **d**, Transfer characteristic recorded at different biases. Inset: The transconductance derived from **d** as a function of $V_g$. **e**, Schematic diagram of the gate effect of cation (red) and anion (blue) distribution within nanochannels and accordingly ionic current modulation.

layer (magenta) serves as a hydrophobic barrier to separate the two HCl solution droplets on either side. Two Ag/AgCl electrodes were directly inserted into both droplets to measure the ionic current. As-calcined thin films were very hydrophobic and usually gave no ionic current above the system noise level (~pA) owing to poor wettability. A 0.1 M HCl solution was first added into the trenches for a day to wet the nanochannels. The films were then rinsed with deionized water several times for ~6 h each before we began ionic conductance measurements. Figure 2b shows a set of representative current/bias ($I/V$) curves at various HCl concentrations. The ionic conductance (the slope of an $I/V$ curve) measured from two mesopore samples is shown in Fig. 2c as a function of nominal $[H^+]$. The dashed lines represent the bulk behaviour of ionic conductance, which is proportional to ionic concentration. However, the measured conductance apparently begins to deviate from bulk behaviour at ~$10^{-1}$–$10^{-2}$ M, exhibits a sharp transition at $10^{-2}$–$10^{-3}$ M and gradually plateaus at lower concentrations. This observation is in part consistent with the emergence of surface-governed unipolar ionic conduction that has been reported previously[7,21], but shows some new characteristics. There is, for example, a sharp transition at $[H^+] \sim 10^{-2}$–$10^{-3}$ M. This can be attributed to the complete protonation of the silica surface, which has a reported isoelectric point of pH 2.6. A slight drop of ionic conductance with increasing proton concentration at the intermediate region ($10^{-5}$–$10^{-3}$ M) probably originates from this surface reaction effect as well. This can be considered as a result of surface-mediated unipolar transport coupled to the protonation of silanol groups on the silica surface. The increased protonation of the silica surface at high HCl concentrations reduces surface charge density and thereby suppresses surface potential.

Under this circumstance, surface charge density is no longer constant even in the unipolar regime. We then conducted an ion transport study using KCl solution to determine the effects of protonation and intrinsic surface charges. The results from the same samples are shown in Fig. 2d. The ionic conductance deviates from the bulk behaviour when the KCl concentration drops below 0.1 M, a condition close to a physiological environment, confirming our expectation that smaller nanochannels lead to a higher upper limit of ionic strength for surface-governed ion transport[18]. However, it usually does not plateau with decreasing KCl concentration, but continues to decrease slightly down to the deionized water level. This is possibly a result of surface charge alteration due to ionic strength change. This observation is in agreement with the ion transport behaviour through a sub-10 nm solid-state nanopore[36], but differs from the distinct two-region ion transport characteristics for large nanochannels[7]. For both proton and potassium ions, the qualitative picture of how the electrical potential profile was altered by ionic concentration is shown in the insets of Fig. 2c,d.

To estimate surface charge density, a semiquantitative analysis is as follows. The total ion density, $n$, can be considered as the sum of two effects: one is the bulk ion density, $2n_0$, whereas the other is the contribution of surface charges, $\sigma \times 2\pi Rl/(F\pi R^2 l) = 2\sigma/FR$, where $n_0$ is the bulk KCl concentration, $\sigma$ is surface charge density, $R$ and $l$ are the diameter and the length of the nanochannels, respectively, and $F$ is the Faraday constant. When

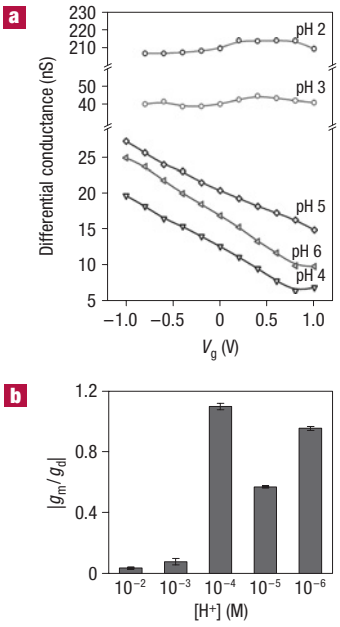


**Figure 4 pH dependence of gate modulation of proton transport. a**, Differential conductance versus $V_g$, derived from the slopes of a set of $I/V$ curves recorded at different pH values. It shows a monotonic modulation of proton conductance at higher pH values (pH = 4, 5 or 6), but much less effect on low pH solutions (pH = 2 or 3). **b**, Ratio of tranconductance to drain conductance, which reveals the capability of gate driving for ionic current relative to direct drain driving at various pH values. Apparently, significant gate control exists only at low proton concentrations where surface- charge-mediated transport dominates.

the ionic conductance begins to deviate from bulk behaviour, the contributions from these two factors are nearly equal, which leads to a simple estimate of surface charge density, $\sigma = n_{0(t)}FR$, where $n_{0(t)}$ is the KCl concentration at the transition point. According to the data collected on four independent mesopore samples, the surface charge density was estimated to be ~0.02–0.07 C m$^{-2}$, which is relatively low compared with those in previous reports[7,18,21].

Significantly, we have further demonstrated that proton transport can be actively modulated through electrostatic gating at low voltages. It has been shown previously that unipolar ion transport through single nanochannels can be electrostatically controlled, but a high voltage (approximately tens of volts) is required and only a modest change can be achieved[18,21]. Here, we design and construct a microfluidic device to interface with much smaller mesopore film patches, which were patterned using a lithography-etching process (see the Supplementary Information). Figure 3a shows a fully integrated mesopore thin-film fluidic device. There are four microfluidic channels fabricated into a silicon-elastomer (polydimethylsiloxane: PDMS) cover chip. In the centre of the device (Fig. 3b), each of these square-mesopore thin-film patches (300–400 μm) is connected by two microfluidic channels. In these patches, aligned mesopores span from one microchannel to the other to create nanofluidic devices. The wet PDMS bonding was used to ensure good sealing and insulation between microfluidic channels. Before bonding, Au electrodes (~100 μm in width), which can be seen in Fig. 3a, were patterned atop the mesopore patches for the application of gate voltage ($V_g$). Ag/AgCl electrodes were inserted into the connecting tubings to measure ionic current. Figure 3c shows a set of representative $I/V$ curves obtained with various gate voltages from −1 to 1 V using a 0.1 mM HCl solution in which zero-shift has been corrected (see the Supplementary Information for single-pore conductance estimation and leakage current consideration). Unambiguously, it exhibits a strong field-effect modulation (up to fourfold) of ionic current. The underlying mechanism for such modulation is similar to that of semiconductor field-effect transistors. Because the electrical potential drop between source and drain electrodes occurs mainly through high-resistance mesoporous films, even higher biases, 5 V, did not cause hydrolysis. The gate voltage has to be sufficiently low so as not to break the dielectrics and the overpotential barrier. In a negatively charged silica mesochannel, cations are the majority carriers determining ionic conductance. A negative electrostatic potential attracts more cations into the mesochannels and consequently enhances the ionic conductance, whereas a positive gate depletes cations and decreases ionic current, analogous to a p-type semiconductor transistor. Figure 3e schematically shows how gate voltages change the cation (red) and ion (blue) distribution in a mesopore film and consequently alter ionic conductance. The selected curves of transfer characteristics, current versus gate voltage, are shown in Fig. 3d for $V = 0.5$ V, 1 V and 1.5 V respectively. They all show consistent p-type gating behaviour. Interestingly, a gate voltage of +1 V was able to completely switch off the apparent ionic current at low biases. This proton transport modulation capability is essential for their potential applications as active media for electrostatic gating of ion/biomolecular transport and manipulation, mimicking biological ion channels. The plot of transconductance, $g_m$, as a function of gate voltage is shown in the inset, which conveys the same message that the negative transconductance is an indication of p-type field-effect modulation. Moreover, the more negative the gate voltages, the more profound modulation can be observed in the experimental range.

To understand the underlying mechanism of proton transport modulation, a systematic study of transport properties under a broad proton concentration range, $10^{-6}$–$10^{-2}$ M, has been conducted. At each proton concentration or pH, a set of $I/V$ curves was recorded with gate voltage ranging from −1 to +1 V. Differential conductance—the slope of an individual $I/V$ curve from a simple linear fit—was extracted and plotted in Fig. 4a. Apparently, the monotonic modulation of conductance by gate voltage is evident only for solutions with a proton concentration of less than $10^{-3}$ M (unipolar ionic region), whereas there is only negligible modulation for high proton concentrations (bipolar ionic region). Interestingly, it is not necessarily at the lowest proton concentrations that we observe the most profound modulation, but usually an intermediate proton concentration (~$10^{-4}$ M) leads to more efficient field-effect control. This is correlated to the proton conductance data shown in Fig. 2c. To better assess the gate modulation efficacy, we extracted the ratio of average transconductance to channel conductance for various proton concentrations. In a simple picture, measured current, $I$, is comprised of the contribution from two components, $I = g_d V_d + g_m V_g$, where $g_d$ is the intrinsic conductance of the channel (also called drain conductance), $g_m$ is the transconductance (also called mutual conductance) acting through capacitive coupling of the gate voltage and the electrostatic potential inside the channels, and $V_d$ and $V_g$ are source/drain bias and gate voltage, respectively. When $V_g = 0$ V, measured current simply equals $g_d V_d$, which allows us to determine $g_d$ at every individual proton concentration. On the basis of this equation, transconductance can be expressed as $g_m = dI/dV_g = V_d dg/dV_g$, where $g$ is the differential conductance calculated on the basis of Fig. 4a. It is assumed that $I/V$ curves adopt a linear mode. For a given bias (for example, 2 V), the absolute values of $g_m/g_d$ at all individual proton concentrations are shown in Fig. 4b. This ratio is a good assessment

of the current driving capability of the gate relative to that of the drain. It is clearly seen that only at low proton concentrations, this ratio is sufficiently large to show gate modulation and the highest $g_m/g_d$ is close to 1.1 at a proton concentration of $\sim 10^{-4}$ M. This result again confirms that the emergence of unique ion transport properties at nanoscales and electrostatic control only arises in systems where surface-charge-governed transport is dominant. We would like to emphasize that the ion conduction in these mesopores (electrophoresis-driven) is fundamentally different from early work on metal nanotubules (diffusion-driven)[16].

In brief, aligned mesoporous silica thin films were used as active media for gated proton transport. Surface-charge-mediated transport was found to dominate at low proton concentrations, whereas bulk-like behaviour emerges right above the isoelectric point of silica surfaces. We have observed two–fourfold proton conduction modulation with a relatively low gate voltage. Such profound electrostatic modulation may have a significant implication in integrated nanofluidic devices for biomolecule manipulation and separation, for example, peptide and amino-acid sorting and identification on the basis of their isoelectric points. It may also find applications in energy conversion, for example, proton-exchange-membrane fuel cells, enzymatically catalysed fuel cells and photoelectrochemical cells.

Received 22 August 2007; accepted 16 January 2008; published 24 February 2008.

## References


1. Decoursey, T. E. Voltage-gated proton channels and other proton transfer pathways. *Physiol. Rev.* **83**, 475–579 (2003).
2. Noji, H., Yasuda, R., Yoshida, M. & Kinosita, K. Direct observation of the rotation of F-1-ATPase. *Nature* **386**, 299–302 (1997).
3. Elston, T., Wang, H. Y. & Oster, G. Energy transduction in ATP synthase. *Nature* **391**, 510–513 (1998).
4. Wang, C. Y. Fundamental models for fuel cell engineering. *Chem. Rev.* **104**, 4727–4765 (2004).
5. Kreuer, K. D. Proton conductivity: Materials and applications. *Chem. Mater.* **8**, 610–641 (1996).
6. Mauritz, K. A. & Moore, R. B. State of understanding of Nafion. *Chem. Rev.* **104**, 4535–4585 (2004).
7. Stein, D., Kruithof, M. & Dekker, C. Surface-charge-governed ion transport in nanofluidic channels. *Phys. Rev. Lett.* **93**, 035901 (2004).
8. Daiguji, H., Yang, P. D. & Majumdar, A. Ion transport in nanofluidic channels. *Nano Lett.* **4**, 137–142 (2004).
9. Pu, Q. S., Yun, J. S., Temkin, H. & Liu, S. R. Ion-enrichment and ion-depletion effect of nanochannel structures. *Nano Lett.* **4**, 1099–1103 (2004).
10. van der Heyden, F. H. J., Bonthuis, D. J., Stein, D., Meyer, C. & Dekker, C. Electrokinetic energy conversion efficiency in nanofluidic channels. *Nano Lett.* **6**, 2232–2237 (2006).
11. van der Heyden, F. H. J., Stein, D., Besteman, K., Lemay, S. G. & Dekker, C. Charge inversion at high ionic strength studied by streaming currents. *Phys. Rev. Lett.* **96**, 224502 (2006).
12. Karnik, R., Duan, C. H., Castelino, K., Daiguji, H. & Majumdar, A. Rectification of ionic current in a nanofluidic diode. *Nano Lett.* **7**, 547–551 (2005).
13. Vlassiouk, I. & Siwy, Z. Nanofluidic diode. *Nano Lett.* **7**, 552–556 (2007).
14. Siwy, Z., Heins, E., Harrell, C. C., Kohli, P. & Martin, C. R. Conical-nanotube ion-current rectifiers: The role of surface charge. *J. Am. Chem. Soc.* **126**, 10850–10851 (2004).
15. Siwy, Z. & Fulinski, A. Fabrication of a synthetic nanopore ion pump. *Phys. Rev. Lett.* **89**, 198103 (2002).
16. Siwy, Z., Kosinska, I. D., Fulinski, A. & Martin, C. R. Asymmetric diffusion through synthetic nanopores. *Phys. Rev. Lett.* **94**, 048102 (2005).
17. Karnik, R., Castelino, K., Fan, R., Yang, P. & Majumdar, A. Effects of biological reactions and modifications on conductance of nanofluidic channels. *Nano Lett.* **5**, 1638–1642 (2005).
18. Karnik, R. *et al.* Electrostatic control of ions and molecules in nanofluidic transistors. *Nano Lett.* **5**, 943–948 (2005).
19. Daiguji, H., Yang, P. D., Szeri, A. J. & Majumdar, A. Electrochemomechanical energy conversion in nanofluidic channels. *Nano Lett.* **4**, 2315–2321 (2004).
20. Goldberger, J., Fan, R. & Yang, P. D. Inorganic nanotubes: A novel platform for nanofluidics. *Accounts Chem. Res.* **39**, 239–248 (2006).
21. Fan, R., Yue, M., Karnik, R., Majumdar, A. & Yang, P. D. Polarity switching and transient responses in single nanotube nanofluidic transistors. *Phys. Rev. Lett.* **95**, 086607 (2005).
22. Nishizawa, M., Menon, V. P. & Martin, C. R. Metal nanotubule membranes with electrochemically switchable ion-transport selectivity. *Science* **268**, 700–702 (1995).
23. Martin, C. R., Nishizawa, M., Jirage, K., Kang, M. S. & Lee, S. B. Controlling ion-transport selectivity in gold nanotubule membranes. *Adv. Mater.* **13**, 1351–1362 (2001).
24. Reisner, W. *et al.* Statics and dynamics of single DNA molecules confined in nanochannels. *Phys. Rev. Lett.* **94**, 196101 (2005).
25. Tegenfeldt, J. O. *et al.* The dynamics of genomic-length DNA molecules in 100-nm channels. *Proc. Natl Acad. Sci. USA* **101**, 10979–10983 (2004).
26. Cao, H. *et al.* Fabrication of 10 nm enclosed nanofluidic channels. *Appl. Phys. Lett.* **81**, 174–176 (2002).
27. Mao, P. & Han, J. Y. Fabrication and characterization of 20 nm planar nanofluidic channels by glass–glass and glass–silicon bonding. *Lab Chip* **5**, 837–844 (2005).
28. Yang, P. D., Zhao, D. Y., Margolese, D. I., Chmelka, B. F. & Stucky, G. D. Generalized syntheses of large-pore mesoporous metal oxides with semicrystalline frameworks. *Nature* **396**, 152–155 (1998).
29. Miyata, H. *et al.* Silica films with a single-crystalline mesoporous structure. *Nature Mater.* **3**, 651–656 (2004).
30. Zhao, D. Y. *et al.* Triblock copolymer syntheses of mesoporous silica with periodic 50–300 angstrom pores. *Science* **279**, 548–552 (1998).
31. Zhao, D. *et al.* Continuous mesoporous silica films with highly ordered large pore structures. *Adv. Mater.* **10**, 1380 (1998).
32. Zhao, D. Y., Sun, J. Y., Li, Q. Z. & Stucky, G. D. Morphological control of highly ordered mesoporous silica SBA-15. *Chem. Mater.* **12**, 275 (2000).
33. Wu, C. W., Ohsuna, T., Edura, T. & Kuroda, K. Orientational control of hexagonally packed silica mesochannels in lithographically designed confined nanospaces. *Angew. Chem. Int. Edn* **46**, 5364–5368 (2007).
34. Wu, C. W., Yamauchi, Y., Ohsuna, T. & Kuroda, K. Structural study of highly ordered mesoporous silica thin films and replicated Pt nanowires by high-resolution scanning electron microscopy (HRSEM). *J. Mater. Chem.* **16**, 3091–3098 (2006).
35. Yamauchi, Y. *et al.* Magnetically induced orientation of mesochannels in 2D-hexagonal mesoporous silica films. *J. Mater. Chem.* **16**, 3693–3700 (2006).
36. Smeets, R. M. M. *et al.* Salt dependence of ion transport and DNA translocation through solid-state nanopores. *Nano Lett.* **6**, 89–95 (2006).


## Acknowledgements

This work was supported by the Air Force Office of Scientific Research, and the Division of Materials Sciences and Engineering, Office of Basic Energy Sciences, Department of Energy.
Correspondence and requests for materials should be addressed to P.Y.
Supplementary Information accompanies this paper on www.nature.com/naturematerials.